# Interfacial organization and phase behavior of mixed galactolipid-DPPC-phytosterol assemblies at the air-water interface and in hydrated mesophases

Jeanne Kergomard, Frédéric Carrière, G. Paboeuf, Franck Artzner, Nathalie Barouh, Claire Bourlieu-Lacanal, V. Vié

## Graphical abstract

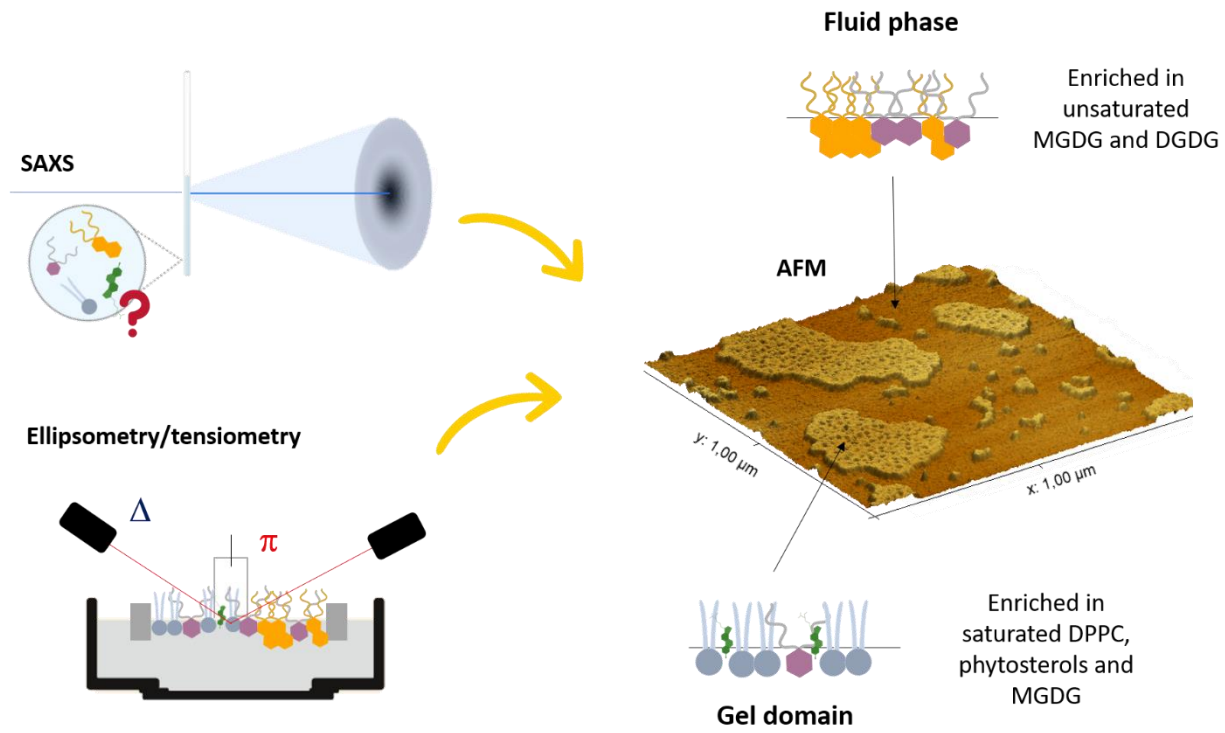


## HIGHLIGHTS

- Plant polar lipids formed stable monolayers at the air/water interface.
- Phytosterols reduced the lateral elasticity of galactolipid and DPPC monolayer.
- DPPC has affected MGDG-DGDG interactions.
- Results highlighted preferential phase miscibility between DPPC and MGDG.

**Title:** Interfacial organization and phase behavior of mixed galactolipid-DPPC-phytosterol assemblies at the air-water interface and in hydrated mesophases

**Name(s) of Author(s)** Jeanne Kergomard[1,2], Frédéric Carrière[3], Gilles Paboeuf[1], Franck Artzner[1], Nathalie Barouh[4,5], Claire Bourlieu[2] & Véronique Vié[1,6]*

**Author Affiliation(s)** [1] IPR Institute of Physics, UMR UR1 CNRS 6251, Rennes 1 University, France; [2]INRAE/CIRAD/UM/Institut Agro Montpellier UMR 1208 IATE, France; [3]Aix-Marseille Université, CNRS, UMR7281 Bioénergétique et Ingénierie des Protéines, Marseille, France ; [4]CIRAD, UMR QUALISUD, F34398 Montpellier-France, [5]Qualisud, Univ Montpellier, Avignon Université, CIRAD, Institut Agro, Université de La Réunion, Montpellier, France ; [6] Univ Rennes 1, CNRS, ScanMAT - UMS 2001, F-35042, Renne, France

*C**orresponding author: Dr. Véronique Vié, Institut de Physique de Rennes, Campus de Beaulieu, UMR UR1 CNRS 6251, Université de Rennes 1, 35042 Rennes cedex,** phone number: 033223235645 and E-mail address : veronique.vie@univ-rennes1.fr

**Present/permanent address:** Institut de Physique de Rennes, campus de Beaulieu, 35042 Rennes cedex – France

**Word count: 6272**

**Total number of tables/figures: 8**

## Abbreviations

AFM: atomic force microscopy

DGDG: digalactosyldiacylglycerol

DPPC: 1,2-dipalmitoyl-sn-glycero-3-phosphocholine

GL: galactolipid

MGDG: monogalactosyldiacylglycerol

PL: phospholipid

pS: phytosterol

PUFA: polyunsaturated fatty acids

SAXS: X-ray scattering

## ABSTRACT

The structural behavior of model assemblies composed of monogalactosyldiacylglycerol (MGDG) and digalactosyldiacylglycerol (DGDG), the two main galactolipids found in plants, was investigated at the air/water interface and in aqueous dispersion. To approach the composition of the natural photosynthetic membranes, tunable Langmuir model membrane of galactolipids (GL) were used, and were complexified to form either heterogenous binary or ternary assemblies of GL, phospholipids (PL), and phytosterols (pS).

The impact of pS, 1,2-dipalmitoyl-sn-glycero-3-phosphocholine (DPPC) or both on the structural properties of GL membrane was studied. The nature of the interactions between the different molecules was investigated using biophysical characterizations (ellipsometry, tensiometry, atomic force microscopy). In addition, the phase behavior was determined by SAXS analysis on the model assemblies in aqueous dispersions.

Results revealed the good interfacial stability of these specific plant membrane lipids. The morphology of the GL film was characteristic of a fluid phase, with an interfacial roughness induced by the intercalation of monogalactosyl and digalactosyl polar heads of MGDG and DGDG, respectively. A phase heterogeneity in the monolayer was induced by the addition of DPPC and/or pS, which resulted in the modification of galactolipid organization and headgroup interactions. These structural changes were confirmed by SAXS analysis, showing more favorable interactions between MGDG and DPPC than between DGDG and DPPC in aqueous dispersion. This phenomenon was exacerbated in the presence of pS.



**KEYWORDS:** galactolipid, phytosterol, natural surfactant, vegetal photosynthetic assemblies

## 1 INTRODUCTION

Galactolipids are the most abundant polar lipids found in higher plants. These glycolipids are actively involved in the structuration of the plant membranes and are particularly concentrated in the photosynthetic chloroplast membranes (80% wt. of total non-pigmented lipids), which contain large amounts of monogalactosyldiacylglycerol (MGDG, 53% wt.) and digalactosyldiacylglycerol (DGDG, 27% wt.) (Gurevich et al., 1997). MGDG possess a small 1-β-galactose polar head bound to a diacylglycerol, giving it a conical shape, which can induce curvatures in lamellar phases (Lee, 2000). On the other hand, DGDG has a larger polar head with an additional α-galactose, linked to β-galactose (Mizusawa & Wada, 2012) and adopts a cylindrical shape in solution. Both GL possess two esterified acyl chains at the *sn*-1 and *sn*-2 position of the glycerol backbone, whose molecular motion depends on the number of unsaturation.

Due to their different structure, MGDG and DGDG exhibit distinct phase behaviors, which govern the overall membrane architecture (Fig. 1). Indeed, studies on the phase behavior of GL have shown that DGDG forms lamellar phases ($L_\alpha$) and induces bilayer formation, whereas unsaturated MGDG tends to form inverted hexagonal structures ($H_{II}$) in aqueous solution (Brentel et al., 1985). In addition to their biological functions in photosynthetic membranes, GL are of nutritional interest since they are rich in polyunsaturated fatty acids (PUFA), and their consumption provides essential ω3 fatty acids (Sahaka et al., 2020).

Phytosterols (pS) are also among the major compounds of photosynthetic plant membranes where they play crucial roles in regulating the physical properties of membranes (Evans, 1991; Ostlund, 2002). More than 250 species of phytosterols have been reported, the most abundant being β-sitosterol (70% wt.), stigmasterol (20% wt.) and campesterol (5% wt.) (Evans, 1991). These pS

in their free form participate in the structuration of membranes by stabilizing polar lipid bilayers, although to a lesser extent than their cholesterol counterpart in animal cell membranes (Moreau et al., 2002). Beyond their structural properties, phytosterols are also compounds of nutritional and medical importance. Their consumption from fruits and vegetables has been shown to lower the total cholesterol and LDL levels in plasma in humans (St-Onge & Jones, 2003). The interesting structural and nutritional properties of GL and pS have raised interest in their use in various applications, which requires a deep understanding of the organization and interactions of these plant polar lipids.

The monolayer behavior of saturated GL has already been extensively studied at the air/water interface (Hoyo et al., 2016; Tomoaia-Cotişel et al., 1989). Nevertheless, it should be noted that GL acyl chains in higher plants are mostly polyunsaturated, and thus less stable since they are more susceptible to oxidation (Tomoala-Cotişel et al., 1983). Monolayer studies have also been performed on GL mixtures with unsaturation indices greater than 1, highlighting the differences in interfacial behavior between saturated and unsaturated GL. Using Langmuir films, Bottier et al. (2007) studied the interfacial behavior of GL from different wheat tissues and highlighted the miscibility of MGDG and DGDG in water but also their tendency to phase separation in mixture. Overall, interface organization and packing were governed by interactions between the sugar polar heads of GL (Bishop et al., 1980), but also depended on their fatty acid composition and the number of unsaturations.

The impact of plant sterols in polar lipid bilayers has already been studied extensively, showing that they alter phase transitions and membrane fluidity (Itzhaki et al., 1990; McKersie & Thompson, 1979), depending on their chemical structure and concentration (Kamal & Raghunathan, 2012). The interactions between pS and dipalmitoylphosphatidylcholine (DPPC)

have also been studied in model Langmuir films at the air/water interface, and the incorporation of β-sitosterol and stigmasterol into PL monolayers has been shown to increase their packing (Su et al., 2007). Nevertheless, to the best of our knowledge, few results are available today concerning the impact of pS and phospholipids on GL interactions and packing in monolayers.

The interfacial properties of MGDG and DGDG, as well as their modulation by DPPC and/or pS in mixed Langmuir monolayers at the air/water interface were studied by ellipsometry, tensiometry and atomic force microscopy (AFM). The phase behavior and physical properties of these mixtures in hydrated mesophases were also studied by small angle X-ray scattering (SAXS)

## 2 EXPERIMENTAL SECTION

### 2.1 Lipids

1,2-dipalmitoylphosphatidylcholine (DPPC), monogalactosyldiacylglycerol (MGDG) and digalactosyldiacylglycerol (DGDG) were purchased from Avanti Polar Lipids (see Table S1 in the supplementary material for the fatty acid repartition). Canola phytosterols were a gift from Cognis France (Estarac, France) obtained from desodorization distillates of canola oil. Typical molar composition (calculated from usual normalized GC procedures) was: β-sitosterol (50 mol%), campesterol (40 mol%) and brassicasterol (10 mol%).

### 2.2. Preparation of multicomponent lipid blends

Simple binary mixture of MGDG and DGDG (60:40, mol/mol) was prepared, namely GL. Ternary and quaternary mixtures of glycerophospholipids, galactolipids and phytosterols (see Table 1 for relative molar composition) were prepared to add some phase heterogeneity and to mimic the composition of natural plant photosynthetic membranes.

### 2.3 Ellipsometry and surface pressure measurements at the air/water interface

All reported experiments were performed at least in duplicate, using a computer controlled and user-programmable LB Teflon Langmuir trough (KSV Nima, Helsinki, Finland) of 77 $cm^2$, equipped with two mobile barriers, allowing to vary the surface. Before each experiment, the trough was carefully cleaned with ultrapure water and ethanol to get rid of the surface-active residual impurities. The surface pressure was measured using a Wilhelmy balance connected to a microelectronic feedback system (Nima Technology, Cambridge, UK). The values of surface pressure ($\pi$) were recorded every 15 s with a precision of 0.2 mN/m. A home-made automated ellipsometer in a "null ellipsometer" configuration was used to carry out the ellipsometric angle

(Δ) measurement (Berge & Renault, 1993). The laser beam probed a surface of 1 $mm^2$ and a depth of 1 µm and allowed the qualitative monitoring of the thickness of the lipid monolayer formed at the air/water interface. Values of Δ were recorded every 15 s with a precision of ± 0.5 °.

### 2.3.1 Formation of the lipid monolayers and Langmuir Blodgett transfer

For all the characterizations, the aqueous phase was composed of a 10 mM Tris HCl buffer solution (100 mM NaCl, 5 mM CaCl2, 10 mM Tris) at pH 7. The monolayers were formed by spreading a few microliters of 1 mM solution of lipids in $CHCl_3$/MeOH (2:1, v/v) at the air/water interface using a Hamilton microliter syringe. The surface area of the Langmuir trough was set at 35 $cm^2$ and the lipids were deposited up to a surface pressure of 20 mN/m. The film was then equilibrated for 10 minutes before each measurement, allowing the evaporation of solvent and lipid organization at the air/water interface. After 10 minutes equilibrium, the interfacial film was transferred onto a freshly cleaved mica plate, using the Langmuir Blodgett method (lipid-transfer ratio ~ 1.0). All lipid layers were sampled at a very low speed (0.5 $mm.min^{-1}$) by raising vertically the mica plate through the air/water interface. The surface pressure was kept constant during the sampling to maintain the lateral organization of lipids and thus avoid desorption phenomena and interfacial disorganization.

### 2.3.2 Compression isotherms and compressibility modulus $C^{-1}$

The surface area of the Langmuir trough was set at 77 $cm^2$ before compression. Few microliters of 1 mM solution of lipids in $CHCl_3$/MeOH (2:1, v/v) were spread at the interface until the pressure reaches 0.1 mN/m. The surface pressure as a function the surface area of the trough (π-A isotherm) was then recorded upon a symmetrical compression of the lipid monolayer using the two barriers, from 77 $cm^2$ to 21 $cm^2$, until the collapse of the film. The barrier speed was set at 5 $mm^2$/min.

Compression isotherms allow to obtain several parameters on the behavior of monolayers under compression. The minimum molecular area corresponds to the mean molecular area occupied by the molecules at the collapse of the film and was calculated as the intercept value between the pressure plateau at collapse and the tangent at the end of the π-A isotherm. The lift-off area was determined as the mean molecular area occupied by the molecules when the pressure begins to increase under compression. Finally, the monolayer compressibility was obtained from the first derivate of π-A isotherm and the mean molecular area of lipids deposited at the interface (Gaines & Prigogine, 1966; Smaby et al., 1997). The equation (1) was used to determine the compressibility coefficient (Cs) of the monolayer.

$$(1)\ Cs = -\frac{1}{A} \times \frac{dA}{d\pi}$$

where π is the surface pressure and A is the mean molecular area of the lipids forming the monolayer, estimated from the surface of the trough and the amounts of lipids deposited. The reciprocal of compressibility coefficient, the compressibility modulus, i.e., $C_s^{-1}$ was represented as a function of the mean molecular area (Å²/molecules). $C_s^{-1}$ values were obtained at equally spaced surface pressures (0.2 mN/m intervals).

### 2.4. Topographic visualization of the monolayer interface using atomic force microscopy

Imaging of the films transferred to mica plates was carried out using an AFM (Multimode Nanoscope 5, Bruker, France). The PeakForce Quantitative Nanomechanical Mapping (QNM in air, 20°C) was used in all the experiments. This mode provides high-resolution AFM images of the sample nanoscale surface topography, as well as the modulus and adhesion, at an acquisition speed comparable to the tapping mode. A standard silicon cantilever was used (0.06 N/m, SNL-10, Bruker, France), and the scan rate was set at 1 Hz. The force was minimized during all scans and

the scanner size was 100×100 µm². The processed images analyzed by the open-source platform Gwyddion are representative of at least duplicated experiments. The differences of height of the LC and LE domains were assessed by the plot of height profile based on three cross-sections of the image using the software Gwyddion (2.55). For all AFM images, the color scale covers a height range of 15 nm, with the darkest color corresponding to the lowest domains and the lightest color to the highest domains, the fluid background corresponding to zero. A color scale is provided in Figure 3 to facilitate interpretation of the images.

### 2.5. Determination of the phase behavior of the model lipid mixture in aqueous dispersions by SAXS

The phase behavior of the model lipid mixture was investigated in aqueous dispersions using X-ray scattering with a homemade set-up at the Rennes Physique Institute. The X-ray scattering results were collected with a Pilatus 300 K (Dectris, Switzerland), mounted on a microsource X-ray generator GeniX 3D (Xenocs, France) operating at 30 W. The monochromatic CuKa radiation was of l = 1.541 Å. The X-ray diffraction patterns were recorded in a reciprocal space q = ($4\pi$. sinθ)/λ from repetitive distances q=0.012 to 1.742 $Å^{-1}$. Small Angle X-ray Scattering (SAXS) and Wide-Angle X-ray Scattering (WAXS) regions were used to determine the supramolecular organization (long range order) of the lipid/water systems and the packing of acyl chains (short range order), respectively. The samples were prepared by evaporation of the solvent containing the solubilized lipids and then hydration at 5% wt of the lipid films in a Tris buffer solution pH 7 (0.5 mg of lipids hydrated in 10 µL of Tris buffer). The samples were then introduced in thin calibrated quartz capillaries (Ø 1.5 mm, GLAS W. Muller, Berlin, Germany) before being centrifuged and sealed with candle wax. For the analysis, they have been introduced in a capillary holder accommodating 19 capillaries at controlled temperature. The homogeneity of the sample was

checked at two y-positions. The analyses were carried out following a heating and cooling temperature ramp from 12 °C to 42 °C and 42 °C to 12 °C, respectively, every 8°C with an exposure time per point of 10 minutes. The results were collected by a homemade program and the positions of Bragg reflections were determined by the Igor Pro 7.0 software (Wavemetrics, US).

## 3 RESULTS AND DISCUSSION

### 3.1 Study of the compression isotherms π-A of the $GL_x/pS_y$ systems – influence of the pS concentration

The absence of shoulder and/or inflection point on the compression isotherm of the GL mixture (Fig. 2.A) was characteristic of a homogeneous liquid-expanded (LE) single phase, which could be explained by the high unsaturation content of the mixture. Indeed, the unsaturations decreased the intensity of van der Walls interactions between the acyl chains, and could hinder the establishment of a tight packing between GL molecules in the monolayer. The isotherm of the GL film indicated a lift-off area at around 230.8 ± 1.8 Å²/molecule (2.3 nm²/molecule) and showed a regular increase of the surface pressure until the collapse of the film at π=39.9 ± 0.2 mN/m and at a limiting area of 81.0 ± 0.6 Å²/molecule (0.8 nm²/molecule). The evolution of the π-A isotherm of the GL film was consistent with the study of Bottier et al. (2007) on purified wheat MGDG and DGDG monolayers, pure or in mixture. Nevertheless, a higher collapse pressure of 47 mN/m had been obtained for the less unsaturated wheat MGDG/DGDG equimolar mixture, at a lower mean molecular area of 70 Å²/molecule (0.7 nm²/molecule). This result was not surprising, as unsaturated acyl chains cannot adopt a very tight packing, which explains a larger average molecular area and a lower surface pressure at collapse as the number of unsaturation increases. The presence of unsaturations in the alkyl chains could also explains the significantly lower $Cs^{-1}_{max}$ which was obtain for the GL monolayer in our study (Fig. 2.B) compared to the $Cs^{-1}_{max}$ reported by Hoyo et al. (2016) on the 2:1 mixture of saturated GL (48 versus 247 mN/m respectively). These values were determined for pressure values of interest, between 30 and 40 mN/m, π=35 mN/m having been proposed as the equivalence surface pressure between lipid monolayers and cellular bilayers (Marsh, 1996, 2007). This decrease in $Cs^{-1}_{max}$ with increasing unsaturation number had also been

reported by Gzyl-Malcher, Filek, Makyła, et al. (2008), reflecting the higher lateral elasticity of unsaturated monolayers compared to the saturated ones.

The addition of pS in the GL mixture did not significantly impact the surface pressure at the collapse of the film (Fig. 2.A). The addition of 5 and 10 mol% pS to the GL mixture did not significantly impact the limiting area. In contrast, the limiting area was affected by the addition of 30 mol% of pS and shifted from 81.0 ± 0.6 to 66.1 ± 0.5 Å²/molecule (0.8 to 0.7 nm²/molecule). The inclusion of pS has also significantly altered the $Cs^{-1}_{max}$ of the monolayers (Fig. 2.B., logarithmic scale), and this effect was particularly marked in the presence of 30 mol% of pS in the GL mixture. Indeed, a $Cs^{-1}_{max}$ of 85.7 mN/m was reached for the $GL_{70}/pS_{30}$ blend, compared to 72.8 mN/m for the $GL_{90}/pS_{10}$ and $GL_{95}/pS_5$ blends and 48.0 mN/m for the pure GL system. The greater impact of phytosterols for a content of 0.3 mol% on the compressibility of the monolayer was consistent with the results presented in Figure 2.D. Indeed, the phase diagram showed a non-ideal behavior of the GL and pS blends, and this effect was even more noticeable for a molar concentration of pS of 30% in the system. The reduction of the mean molecular area at collapse and the increase of $Cs^{-1}_{max}$ with the increase of pS concentration could be attributed either to the condensation of the unsaturated acyl chains or to the reorientation of the sugar polar heads, induced by the presence of the pS molecule, thus decreasing the lateral elasticity of the monolayers (Li et al., 2001). Indeed, the presence of a largely hydrophobic small molecule such as pS will also impact the tilt of the polar heads, which will increase the possibility of packing of the molecules, explaining the non-ideal behavior observed in the case of unsaturated GL monolayers. Nevertheless, the animal counterpart of pS, the cholesterol, was shown to establish weaker interactions with unsaturated lipids, in comparison with saturated lipids (Silvius, 2003), so the

addition of DPPC in the mixtures could drastically alter the phenomena observed in GL-pS monolayers (Jurak, 2013).

### 3.2 Influence of GL, DPPC, and pS interfacial composition on collapse pressure and ellipsometric angle values

Ellipsometry combined with tensiometry were used on Langmuir trough to determine the values of surface pressure ($\pi$, mN/m), ellipsometric angle ($\Delta$, °) and limiting molecular area (Å²/molecule) at the collapse of mixed heterogenous films with various compositions in GL, DPPC and pS. The values of $\pi$ and $\Delta$ at the collapse of the films are presented in Table 2.

The addition of 10 mol% of pS in the GL mixture has induced a clear increase in the film thickness at collapse (8.2 versus 7.3 ± 0.5° for the $GL_{90}/pS_{10}$ versus GL mixture, respectively), while there was no significant change in collapse pressure, neither in the limiting area. These results tend to indicate that the inclusion of the pS only impacted the orientation of the GL sugar polar heads, and not the acyl chain organization.

The addition of 50 mol% DPPC in the GL mixture led to an increase of the collapse surface pressure to $\pi$=44.1 ± 0.2 mN/m (versus 39.9 ± 0.2 mN/m for the GL monolayer) as well as a shift in the mean molecular area at collapse to 60.4 ± 1.0 Å²/molecules (0.6 nm²/molecule), versus 81.0 ± 0.6 Å²/molecule (0.8 nm²/molecule) for the GL monolayer. These results indicated a strong condensing effect of DPPC, which could be explained by the presence of saturated acyl chains and smaller polar head of DPPC, which decreased the steric hindrance. An increase in the film thickness at collapse induced by the presence of DPPC was also observed ($\Delta$=8.9° vs 7.30° for the GL film), suggesting a reorientation of the sugar polar heads of GL, as well as the formation of condensed domains upon compression (Vié et al., 1998).

The addition of phytosterols at 10 mol% in the GL/DPPC film did not induce a significative variation of the collapse pressure (44.4 ± 0.2 mN/m versus 44.1 mN/m for the GL/DPPC) but triggered a shift of the limiting molecular area from 60.4 ± 1.0 to 55.0 ± 1.7 Å²/molecule (0.6 to 0.5 nm²/molecule), indicating an increase of the packing in the mixture in presence of pS. This decrease in the limiting area was not expected, given that pS probably interacts preferentially with DPPC than with PUFA-containing GL. Indeed, Botet-Carreras et al. (2019) have studied the impact of cholesterol on homo- and hetero-acids phospholipid monolayers by AFM and AFM-FS, confirming that the effect of cholesterol on unsaturated PL was weaker than the one exerted on saturated PL. Additionally, a variety of biophysical measurements have revealed that sterols have an aversion to PUFA (Huster et al., 1998; Niu & Litman, 2002; Pitman et al., 2004; Wassall et al., 2004), explaining the lower impact of pS in the presence of GL in the $GL_{90}/pS_{10}$ mixture, which contain a significant amount of PUFA. One possible explanation for such aversion of sterols for PUFA is the high disorder of PUFA acyl chains, which is incompatible with the usual orientation of cholesterol vertically with respect to interface plane. Thus, one can expect a change in the orientation of the sterol backbone (Harroun et al., 2006). Additionally, cholesterol has already been shown to induce order in lipids in fluid phase, whereas it has the opposite effect on lipids present in gel phase (Garcia-Manyes et al., 2010). Given these general effects of sterols and their aversion to PUFA, we were expected a more pronounced disorganization of DPPC molecules than a condensation effect of GL polyunsaturated lipid chains, and thus a larger limiting area for the $GL_{45}/DPPC_{45}/pS_{10}$ mixture compared to the $GL_{50}/DPPC_{50}$ mixture. Nevertheless, given the decrease in the limiting area of the mixture in the presence of pS, it is likely that the addition of pS induced GL organization in the presence of DPPC, raising the question of a potential miscibility between DPPC and MGDG and/or DGDG in the presence of pS, reflecting a more complex mixture.

### 3.3. Characterization by ellipsometry of interfacial films at 20 mN/m

The thickness of the three model systems was determined by ellipsometry at a surface pressure of 20 mN/m. The detailed molar compositions are given in Table 1. The values of ellipsometric angles obtained at 20 mN/m are presented in Table 3. Eight sub-model systems were also prepared to give a better understanding of the organization and interactions between polar lipids at the air/water interface (see supplementary data S1 for the detailed molar compositions and S2 for the ellipsometric angle values at 20 mN/m).

An ellipsometric angle of 7.5° was obtained for the mixed GL monolayer at 20 mN/m., which was identical to the value obtained with DGDG alone and higher than the value for MGDG (7.5 and 6.3 ± 0.5° respectively). This result was expected as the DGDG lipid film has already been shown to be thicker than the MGDG monolayer (Bottier, 2006).

The addition of DPPC to GL at a molar fraction of 0.5 did not induce a significant variation in the thickness at 20 mN/m. This result was consistent with the data obtained with the sub-model systems $MGDG_{50}/DPPC_{50}$ and $DGDG_{50}/DPPC_{50}$ (6.3 and 7.4 ± 0.5°, respectively), in which the addition of DPPC did not induce a significant variation of the ellipsometric angle at 20 mN/m.

The addition of pS to the mixed model system of GL and DPPC, at a molar content of 10%, led to a slight decrease of the ellipsometric angle at 20 mN/m, but it was not significant. By comparison, pS induced a clear decrease in the thickness of the $MGDG_{45}/DPPC_{45}/pS_{10}$ and $DGDG_{45}/DPPC_{45}/pS_{10}$ sub-model systems (5.5 and 6.0 ± 0.5°, respectively), compared to the $MGDG_{50}/DPPC_{50}$ and $DGDG_{50}/DPPC_{50}$ systems (6.3 and 7.4 ± 0.5°, respectively). However, no significant variation in thickness was obtained for the sub-models $MGDG_{90}/pS_{10}$ and

$DGDG_{90}/pS_{10}$, in comparison with the pure MGDG and DGDG systems. These results tend to indicate different interactions of pS with GL-DPPC mixed films and pure MGDG and DGDG.

In order to better understand the differences in the organization of the different models and sub-models, atomic force microscopy was used to visualize the interface of the films obtained by Langmuir Blodgett sampling.

### 3.4 Nanoscale topographic visualization of interfacial films at 20 mN/m using atomic force microscopy

Figure 3 shows AFM images of the interfacial organization of the three main model monolayers GL, $GL_{50}/DPPC_{50}$, and $GL_{45}/DPPC_{45}/pS_{10}$ after their transfer by the Langmuir-Blodgett technique onto a mica plate and at a surface pressure of 20 ± 0.5 mN/m. The scale used was composed of different shades of brown, related to the differences in height in the monolayers. These color variations were correlated with the different tilt values of the lipid molecules and thus provide information on the orientation of the molecules and their physical state.

The 5×5 µm² AFM image of the GL system (Fig. 3.A), was characteristic of a homogeneous liquid-expanded (LE) phase without phase separation, consistent with the presence of unsaturated acyl chains in the fluid phase. However, the 1×1 µm² image highlights the presence of surface roughness, with height differences between 2 to 8 Å (0.2 to 0.8 nm) with respect to the baseline. A similar segregation was previously observed by AFM on mixed films of MGDG:DGDG (68:32 mol/mol) by Sarkis et al. (2014). Additionally, Bottier et al. (2007) had observed the presence of irregular protrusions of 7 Å (0.7 nm) and 4 Å (0.4 nm) at surface pressures above 25 mN/m on monolayers of pure MGDG or in equimolar mixture with DGDG, respectively. The presence of these protrusions had been attributed to a specific organization of the MGDG polar heads between

344 them or with those of DGDG, this roughness being absent on the AFM images of the DGDG
345 monolayer. Indeed, a particular orientation of DGDG polar heads induced by the interactions
346 between GL had been highlighted by PM-IRRAS data. The assumption was that the
347 monogalactosyl polar head of MGDG could be responsible for the orientation of the digalactosyl
348 group of DGDG parallel to the interface, with the formation of a network of hydrogen bridges
349 between the polar heads and the water molecules at the interface (Kanduc et al., 2017).

350 The addition of DPPC to the system (2) (Fig. 3.B) resulted in the appearance of 1 nm high
351 condensed domains of varying shapes and sizes at the interface (5x5 µm² image), likely to be
352 enriched in DPPC, given their degree of saturation. Additionally, a loss of the granularity on 1x1
353 µm² images suggests changes in the orientation of the galactosyl polar heads of GL, that could
354 result from a modification by DPPC of the interactions between MGDG and DGDG. This would
355 fit with the previous results obtained on the compressibility of the film.

356 The addition of pS to the $GL_{50}/DPPC_{50}$ mixture (Fig. 3.C) resulted in a subsequent dilution
357 of the domains in the LC condensed phase, as well as a significant increase in the thickness of the
358 domains (h=1.6 nm versus h=1.0 nm, with and without pS, respectively), in contrast to the
359 unchanged value of the ellipsometric angle. The irregular domain boundaries also indicated a
360 change in line tension induced upon addition of pS in the GL/DPPC system, and suggests a change
361 in interactions between the different classes of lipids, with miscibility regions between the different
362 components. Defects were also visible at the condensed phase domains, probably induced by the
363 inclusion of pS and the local subsequent disorganization of the saturated acyl chains of DPPC.

364 In order to investigate the composition of the condensed phase domains and to better
365 understand the interactions involved between the different classes of lipids, four sub-model systems
366 were prepared, namely $MGDG_{50}/DPPC_{50}$, $DGDG_{50}/DPPC_{50}$, $MGDG_{30}/DPPC_{60}/pS_{10}$ and

$DGDG_{30}/DPPC_{60}/pS_{10}$ (mol%) mixtures. AFM images and height profiles of these sub-models are presented Figure 4.

In the absence of pS, the 5×5 µm² AFM image of the $MGDG_{50}/DPPC_{50}$ mixture (Fig. 4.A) showed the presence of LC phase domains (average domain area=0.1 µm²), of irregular shape and 1.7 nm height, as well as a background characteristic of a homogeneous fluid phase. The $DGDG_{50}/DPPC_{50}$ film (Fig. 4.B) presented a similar fluid background. However, the LC phase domains are more abundant but smaller (average domain area=0.0002 µm²), and present a greater height of 1.9 nm, in accordance with the higher ellipsometric angle for this mixture (6.3° versus 7.4° for the $MGDG_{50}/DPPC_{50}$ and $DGDG_{50}/DPPC_{50}$ mixtures, respectively). These observations confirm the different nature of MGDG and DGDG interactions with DPPC and question a possible segregation of MGDG-DGDG interactions in the presence of DPPC.

The addition of pS up to 10 mol% in these two previous sub-model systems changed the appearance of the interfacial films. First, the addition of pS in the MGDG/DPPC system (Fig. 4.C) induced a change in the line tension of the condensed phase domains, which showed irregular edges as well as the presence of defects at the larger domains, probably induced by the presence of pS, similar to the previous observations on the model systems. Nevertheless, a significant decrease of 18% in the height of these domains (1.7 nm vs. 1.4 nm in height, without and with pS, respectively) was observed, consistent with the evolution of the ellipsometric angle (6.3° vs. 5.5°, without and with pS, respectively). The addition of pS in the DGDG/DPPC mixture induced a similar evolution of the interface (Fig. 4.D): the line tension and the thickness of the condensed domains were also modified according to the same trend (16% decrease in thickness), and the presence of defects at the larger domains with irregular edges was still visible. This change in thickness did not showed

the same trend as that observed in the $GL_{45}/DPPC_{45}/pS_{10}$ model, for which a 45% increase in domain thickness was observed.

Overall, the results confirm the hypotheses of a different miscibility between DPPC and MGDG and between DPPC and DGDG. Moreover, it seems that the inclusion of pS in the systems induced, on the one hand, a transition from the DPPC-enriched gel phase to a less ordered phase, with the apparition of defects, and on the other hand, a transition from a fluid phase to a less ordered zone, with reduced height mismatch and a decrease of the line tension in the ternary systems. To validate these hypotheses and determine the miscibility of DPPC in mixture with MGDG or DGDG, as well as the impact of pS in GL/DPPC lipid systems, SAXS experiments were performed, in the presence of water in excess.

### 3.5. Phase behavior of mixed galactolipid mixtures in hydrated mesophase (SAXS)

The three-dimensional structures of unsaturated MGDG and DGDG, alone or in their equimolar mixture, have already been studied by analysis of the X-ray diffraction patterns and electron density profile at 20°C in excess of water (Bottier et al., 2007; Hoyo et al., 2016). On one hand, the lamellar structure $L_\alpha$ of DGDG was evidenced by the presence of single peaks regularly spaced, with a lamellar periodicity of 54.9 Å. On the other hand, the X-ray diffraction profile obtained for MGDG showed six Bragg diffraction pics, with a hexagonal periodicity of 67.2 Å, that were attributed to an inverse hexagonal phase ($H_{II}$) distribution, which has been observed in other studies over a wide temperature range (-15 to 80°C) (Popova & Hincha, 2011). The ability of unsaturated MGDG to form non-lamellar structures can be neutralized by mixing it with at least 50% of lipids forming lamellar phases. However, unsaturated MGDG can induce defects in the lamellar structure of MGDG/lipid mixtures forming bilayers when its proportion is between 20 and 50% (Castro et al., 2007). Nevertheless, for the equimolar mixture of MGDG and DGDG in excess of water, the SAXS diffraction pattern obtained by Bottier et al. was the signature of a bicontinuous cubic phase (*Im3m* space group) with a cubic lattice parameter of 202 Å, showing the specific behavior of MGDG and DGDG in the equimolar mixture compared to the pure lipids. Indeed, the formation of an *Im3m* space group could result from specific interactions between the polar sugar heads of the MGDG and DGDG.

The three-dimensional organization of DPPC has also already been extensively studied by SAXS, showing a well-ordered multilayer structure in excess of water due to the so-called $L_\beta$ gel phase at 20°C (Et-Thakafy et al., 2017; Varga et al., 2007). Nevertheless, the miscibility of the mixture of GL with DPPC forming lamellar phases has never been studied by SAXS.

First of all, the present study investigated the three-dimensional organization of heterogenous $GL_x/DPPC_y$ mixtures in excess of water, and as a function of DPPC proportion. Figure 5.A presented the X-Ray diffraction patterns of three mixtures of $GL_x/DPPC_y$ in water, with DPPC at 66 (black curve), 50 (blue curve), and 33 mol% (green curve), respectively. The results showed that DPPC in large amount of 66 mol% induced a segregation between the components in water. Indeed, on the diffraction pattern (black line), the large diffraction peaks visible at 0.09 and 0.18 $Å^{-1}$ were identified as the ones related to the $L_\beta$ phase formed by pure DPPC at 20°C. Additionally, a peak and a shoulder were visible on the diffraction pattern at 0.06 and 0.11 $Å^{-1}$, respectively, that could correspond to the diffraction pattern of the cubic phase of the MGDG-DGDG mixture in water, consistent with the results of Bottier et al. (2007). These results tend to indicate a segregation between DPPC and the MGDG-DGDG mixture in water, leading to the existence of two non-miscible phases. Nevertheless, DPPC may also have disrupted the cubic phase by diluting the MGDG-DGDG interactions, coinciding with the distorted pattern of the MGDG-DGDG cubic phase. When DPPC was added at 50 mol% in the GL mixture, the diffraction pattern (blue line) showed a better miscibility between the three components of the system. Indeed, the intensity of the peaks presumably related to the cubic phase of the GL mixture was decreased and the pic 0.06 $Å^{-1}$ was no longer visible, tending to show the existence of two miscible phases. These results were consistent with AFM images of the $GL_{50}DPPC_{50}$ mixture, where a fluid phase was visible, probably composed of a mixture of MGDG, DGDG and DPPC, as well as condensed domains, likely enriched in DPPC. At a ratio of 33 mol% DPPC, the diffraction pattern (green line) indicates that the concentration of DPPC was not sufficient enough to segregate the three components of the system, and the slightly weaker MGDG-DGDG interactions have probably prevailed, leading to the existence of a single organized phase composed by MGDG, DGDG and

DPPC. Overall, the SAXS data confirm the presence of significant segregation in the systems, depending on the DPPC proportion and implying the existence of very selective interactions between the different types of lipids.

To our knowledge, this study is the first on the impact of pS on heterogenous model plant membranes, while the impact of cholesterol on model of animal membranes made of phospholipid bilayers has been extensively studied. To better understand the impact of pS and the interactions between DPPC and MGDG/DGDG, the SAXS diffraction patterns of three other model systems were studied, *i.e.* $MGDG_{45}DPPC_{45}pS_{10}$, $GL_{45}/DPPC_{45}/pS_{10}$ and $DGDG_{45}/DPPC_{45}/pS_{10}$ (fig. 5.B).

On one hand, results tend to show that MGDG and DGDG did not interact equivalently with the DPPC-pS mixture. First of all, the mixture of DGDG with DPPC-pS did not promote the presence of a single organized phase in water (see green line). Indeed, the diffraction pattern of the pure DPPC was clearly visible, with the $L_\beta$ lamellar phase peaks at 0.09, 0.18, and 0.27 $Å^{-1}$. The diffraction pattern of the pure DGDG was also clearly evidenced, with the diffraction peaks reflecting the $L_\alpha$ phase at 0.11 and 0.22 $Å^{-1}$. These results are consistent with those obtained by Bottier et al. (2007) on the wheat DGDG/water system and they highlight the poor miscibility of DGDG with DPPC-pS system. On the contrary, in the case of the $MGDG_{45}/DPPC_{45}/pS_{10}$ mixture (blue pattern), only one phase was clearly visible, with two peaks reflecting a lamellar phase at 0.09 and 0.18 $Å^{-1}$, but slightly shifted compared to pure DPPC in water. In the case of the $GL_{45}/DPPC_{45}/pS_{10}$ mixture in water (black pattern), a shoulder was also visible at 0.11 $Å^{-1}$, compared to the diffraction pattern of the $MGDG_{45}/DPPC_{45}/pS_{10}$ mixture, highlighting the formation of two phases: one phase enriched in MGDG-DPPC-pS and one phase containing a mixture of MGDG-DGDG. These results showed drastically different interactions between MGDG

and DGDG, respectively, and the DPPC-pS mixture, and highlight the preferential miscibility of MGDG with the DPPC-pS mixture.

On the other hand, the comparison between the $GL_{50}/DPPC_{50}$ (fig. 5. A, blue pattern) and the $GL_{45}/DPPC_{45}/pS_{10}$ (fig. 5. B, black pattern) mixtures in water allowed us to highlight the impact of 10 mol% of pS in the system. As expected, pS did not formed a phase on its own but triggered a modification of the organization of the existing phases. Indeed, the inclusion of pS in the GL/DPPC system did not induce the appearance of new diffraction peaks, but has led to a contraction of the $L_\beta$ diffraction peaks at 0.09 and 0.18 $Å^{-1}$, indication a homogenization in the miscibility of the two phases.

Overall, the results were consistent with the AFM images obtained on the $GL_{45}/DPPC_{45}/pS_{10}$ monolayer, with the visualization of a fluid phase composing the background, probably enriched in MGDG-DGDG, and the presence of a gel phase enriched in MGDG-DPPC, in which the inclusion of pS has induced the formation of defects, leading to a thickening of the gel phase by decreasing the packing. Additionally, the observation of smaller domains in presence of pS on the AFM images was consistent with a lowering of the line tension at the edges of the gel domains, resulting from a better miscibility between the two phases and thus a reduced height mismatch.

## CONCLUSION

In this study, tunable Langmuir model membrane of heterogenous assemblies of GL, DPPC and pS were used to study the structural behavior of the main polar lipids of vegetal photosynthetic membrane (MGDG and DGDG) at the air/water interface. The impact of pS and 1,2-dipalmitoyl-sn-glycero-3-phosphocholine (DPPC) or both on the structural properties of GL membrane was studied.

The biophysical results obtained confirmed the good surfactant properties of these polar lipids. The addition of pS in the mixed GL systems up to 30 mol% induced a reorientation of the sugar polar heads, leading to a more important packing and thus to a reduction of the lateral elasticity of the monolayer. The study of the compressibility isotherms of the different films also allowed to highlight the complex miscibility of the heterogeneous ternary mixtures, and their singular behavior compared to the pure systems. Indeed, the results obtained on the $GL_{45}/DPPC_{45}/pS_{10}$ mixture indicated preferential DPPC-pS interactions but a decrease in lateral elasticity despite the disorganization effect of pS on saturated lipids.

The inclusion of pS into the gel phase regions was visible on the AFM images, leading to a thickening of the domains and a local decrease of packing by the appearance of defects. This result highlighted phase miscibility between DPPC and GL, and in particular with MGDG, which was confirmed by AFM images and SAXS diffraction patterns. The favorable interaction between DPPC and pS may have caused the appearance of segregated zones, on one side, devoid of pS and enriched in MGDG-DGDG in the fluid phase, and on the other, enriched in pS and DPPC.

The pS-DPPC-rich areas could also have included the presence of MGDG, due to more favorable DPPC-MGDG interactions than DPPC-DGDG, raising the hypothesis of a heterogeneous MGDG-

507 DPPC-pS composition of the gel phase domains. The characterization of these kinds of plant lipid
508 mixtures is useful for the understanding of mechanisms such as their digestion by specific digestive
509 enzymes.

## Declaration of Competing Interest

The authors declare that they have no known competing financial interests or personal relationships that could have appeared to influence the work reported in this paper.


## Acknowledgments

The authors would like to acknowledge the BIOMIF platform ('Biological Molecules at fluid interfaces', IPR, Rennes, France) for allowing the biophysical characterization of samples presented in this article.

C. Bourlieu, V. Vié and J. Kergomard determined the outline and the content of the manuscript. J. Kergomard wrote the manuscript and all the co-authors participated in the experimental design, the collection, the interpretation of data and the correction and implementation of the manuscript. All co-authors have approved the final article.

## References


Berge, B., & Renault, A. (1993). Ellipsometry Study of 2D Crystallization of 1-Alcohol Monolayers at the Water Surface. *Europhysics Letters (EPL), 21*(7), 773-777. https://doi.org/10.1209/0295-5075/21/7/010

Bishop, D. G., Kenrick, J. R., Bayston, J. H., Macpherson, A. S., & Johns, S. R. (1980). Monolayer properties of chloroplast lipids. *Biochimica et Biophysica Acta (BBA) - Biomembranes, 602*(2), 248-259. https://doi.org/10.1016/0005-2736(80)90308-9

Botet-Carreras, A., Montero, M. T., Domènech, Ò., & Borrell, J. H. (2019). Effect of cholesterol on monolayer structure of different acyl chained phospholipids. *Colloids and Surfaces B: Biointerfaces, 174*, 374-383. https://doi.org/10.1016/j.colsurfb.2018.11.040

Bottier, C. (2006). *Caractérisation des puroindolines, des galactolipides du blé et de leurs interactions : Mesures physiques aux interfaces* [Phdthesis, Université Rennes 1]. https://tel.archives-ouvertes.fr/tel-00148405

Bottier, C., Géan, J., Artzner, F., Desbat, B., Pézolet, M., Renault, A., Marion, D., & Vié, V. (2007). Galactosyl headgroup interactions control the molecular packing of wheat lipids in Langmuir films and in hydrated liquid-crystalline mesophases. *Biochimica Et Biophysica Acta, 1768*(6), 1526-1540. https://doi.org/10.1016/j.bbamem.2007.02.021

Brentel, I., Selstam, E., & Lindblom, G. (1985). Phase equilibria of mixtures of plant galactolipids. The formation of a bicontinuous cubic phase. *Biochimica et Biophysica Acta (BBA) - Biomembranes, 812*(3), 816-826. https://doi.org/10.1016/0005-2736(85)90277-9

Castro, V., Dvinskikh, S. V., Widmalm, G., Sandström, D., & Maliniak, A. (2007). NMR studies of membranes composed of glycolipids and phospholipids. *Biochimica et Biophysica Acta*

*(BBA) - Biomembranes*, *1768*(10), 2432-2437. https://doi.org/10.1016/j.bbamem.2007.05.010

Et-Thakafy, O., Delorme, N., Gaillard, C., Mériadec, C., Artzner, F., Lopez, C., & Guyomarc'h, F. (2017). Mechanical Properties of Membranes Composed of Gel-Phase or Fluid-Phase Phospholipids Probed on Liposomes by Atomic Force Spectroscopy. *Langmuir*, *33*(21), 5117-5126. https://doi.org/10.1021/acs.langmuir.7b00363

Evans, C. S. (1991). J. B. Harborne (ED.) Methods in plant biochemistry : 1. plant phenolics. Academic Press, New York and London, 1990. *Phytochemical Analysis*, *2*(1), 48-48. https://doi.org/10.1002/pca.2800020110

Gaines, G. L., & Prigogine, I. P. (1966). *Insoluble monolayers at liquid-gas interfaces*.

Garcia-Manyes, S., Redondo-Morata, L., Oncins, G., & Sanz, F. (2010). Nanomechanics of Lipid Bilayers : Heads or Tails? *Journal of the American Chemical Society*, *132*(37), 12874-12886. https://doi.org/10.1021/ja1002185

Gurevich, V., Bondarenko, B., Gundermann, K. J., Schumacher, R., Astashkina, T., Ivanov, V., Popov, Y., Shatilina, L., & Kazennova, N. (1997). Poly-unsaturated phospholipids increase the hypolipidemic effect of Lovastatin. *European Journal of Internal Medicine*, *8*(1), 15-20.

Gzyl-Malcher, B., Filek, M., Makyła, K., & Paluch, M. (2008). Differences in surface behaviour of galactolipoids originating from different kind of wheat tissue cultivated in vitro. *Chemistry and Physics of Lipids*, *155*(1), 24-30. https://doi.org/10.1016/j.chemphyslip.2008.06.004

Hoyo, J., Guaus, E., & Torrent-Burgués, J. (2016). Monogalactosyldiacylglycerol and digalactosyldiacylglycerol role, physical states, applications and biomimetic monolayer films. *The European Physical Journal E*, *39*(3), 39. https://doi.org/10.1140/epje/i2016-16039-0

Itzhaki, H., Borochov, A., & Mayak, S. (1990). Age-Related Changes in Petal Membranes from Attached and Detached Rose Flowers. *Plant Physiology*, *94*(3), 1233-1236.

Jurak, M. (2013). Thermodynamic Aspects of Cholesterol Effect on Properties of Phospholipid Monolayers : Langmuir and Langmuir–Blodgett Monolayer Study. *The Journal of Physical Chemistry B*, *117*(13), 3496-3502. https://doi.org/10.1021/jp401182c

Kanduc, M., Schlaich, A., de Vries, A. H., Jouhet, J., Marechal, E., Deme, B., Netz, R. R., & Schneck, E. (2017). Tight cohesion between glycolipid membranes results from balanced water-headgroup interactions. *Nature Communications*, *8*, 14899. https://doi.org/10.1038/ncomms14899

Lee, A. G. (2000). Membrane lipids : It's only a phase. *Current Biology*, *10*(10), R377-R380. https://doi.org/10.1016/S0960-9822(00)00477-2

Li, X.-M., Momsen, M. M., Smaby, J. M., Brockman, H. L., & Brown, R. E. (2001). Cholesterol Decreases the Interfacial Elasticity and Detergent Solubility of Sphingomyelins. *Biochemistry*, *40*(20), 5954-5963. https://doi.org/10.1021/bi002791n

Marsh, D. (1996). Lateral pressure in membranes. *Biochimica et Biophysica Acta (BBA) - Reviews on Biomembranes*, *1286*(3), 183-223. https://doi.org/10.1016/S0304-4157(96)00009-3

Marsh, D. (2007). Lateral Pressure Profile, Spontaneous Curvature Frustration, and the Incorporation and Conformation of Proteins in Membranes. *Biophysical Journal*, *93*(11), 3884-3899. https://doi.org/10.1529/biophysj.107.107938

McKersie, B. D., & Thompson, J. E. (1979). Influence of Plant Sterols on the Phase Properties of Phospholipid Bilayers 1. *Plant Physiology*, *63*(5), 802-805.

Mizusawa, N., & Wada, H. (2012). The role of lipids in photosystem II. *Biochimica et Biophysica Acta (BBA) - Bioenergetics*, *1817*(1), 194-208. https://doi.org/10.1016/j.bbabio.2011.04.008

Moreau, R. A., Whitaker, B. D., & Hicks, K. B. (2002). Phytosterols, phytostanols, and their conjugates in foods : Structural diversity, quantitative analysis, and health-promoting uses. *Progress in Lipid Research*, *41*(6), 457-500. https://doi.org/10.1016/s0163-7827(02)00006-1

Popova, A. V., & Hincha, D. K. (2011). Thermotropic phase behavior and headgroup interactions of the nonbilayer lipids phosphatidylethanolamine and monogalactosyldiacylglycerol in the dry state. *BMC Biophysics*, *4*(1), 11. https://doi.org/10.1186/2046-1682-4-11

Sahaka, M., Amara, S., Wattanakul, J., Gedi, M. A., Aldai, N., Parsiegla, G., Lecomte, J., Christeller, J. T., Gray, D., Gontero, B., Villeneuve, P., & Carrière, F. (2020). The digestion of galactolipids and its ubiquitous function in Nature for the uptake of the essential α-linolenic acid. *Food & Function*. https://doi.org/10.1039/D0FO01040E

Sarkis, J., Rocha, J., Maniti, O., Jouhet, J., Vié, V., Block, M. A., Breton, C., Maréchal, E., & Girard-Egrot, A. (2014). The influence of lipids on MGD1 membrane binding highlights novel mechanisms for galactolipid biosynthesis regulation in chloroplasts. *The FASEB Journal*, *28*(7), 3114-3123. https://doi.org/10.1096/fj.14-250415

Silvius, J. R. (2003). Role of cholesterol in lipid raft formation : Lessons from lipid model systems. *Biochimica Et Biophysica Acta*, *1610*(2), 174-183. https://doi.org/10.1016/s0005-2736(03)00016-6

Smaby, J. M., Momsen, M. M., Brockman, H. L., & Brown, R. E. (1997). Phosphatidylcholine acyl unsaturation modulates the decrease in interfacial elasticity induced by cholesterol. *Biophysical Journal*, *73*(3), 1492-1505. https://doi.org/10.1016/S0006-3495(97)78181-5

St-Onge, M.-P., & Jones, P. J. H. (2003). Phytosterols and human lipid metabolism : Efficacy, safety, and novel foods. *Lipids*, *38*(4), 367-375. https://doi.org/10.1007/s11745-003-1071-3

Su, Y., Li, Q., Chen, L., & Yu, Z. (2007). Condensation effect of cholesterol, stigmasterol, and sitosterol on dipalmitoylphosphatidylcholine in molecular monolayers. *Colloids and Surfaces A: Physicochemical and Engineering Aspects*, *293*(1), 123-129. https://doi.org/10.1016/j.colsurfa.2006.07.016

Tomoaia-Cotişel, M., Zsako, J., Chifu, E., & Quinn, P. J. (1989). Hysteresis in compression-expansion cycles of distearoylmonogalactosylglycerol monolayers. *Chemistry and Physics of Lipids*, *50*(2), 127-133. https://doi.org/10.1016/0009-3084(89)90036-4

Varga, Z., Bóta, A., & Goerigk, G. (2007). Localization of dihalogenated phenols in vesicle systems determined by contrast variation X-ray scattering. *Journal of Applied Crystallography*, *40*(s1), s205-s208. https://doi.org/10.1107/S0021889807001987

## FIGURES

Figure captions.

**Figure 1** Molecular structure and phase behaviour of A) monogalactodiacylglycerol (MGDG) and B) digalactosyldiacylglycerol (DGDG). Lα standing for lamellar phase and HII standing for hexagonal inverted phase.

**Figure 2** Compression isotherms of 1) GL (red), 2) $GL_{95}/pS_5$ (deep blue), 3) $GL_{90}/pS_{10}$ (green), 4) $GL_{70}/pS_{30}$ (black) monolayers at the air/water interface. A) The graph corresponds to the evolution of π (mN/m) as a function of the mean molecular area (Å²/molecules). B) The graph corresponds to the evolution of the surface compressibility moduli ($C_s^{-1}$, calculated following the equation (1)), as a function of π (mN/m) of 1), 2), 3) and 4). C) The graph corresponds to the evolution of π (mN/m) as a function of the mean molecular area (Å²/molecules) of the pure pS system. D) The graph corresponds to the mean molecular area (Å²/molecules) at 20 mN/m of each monolayer as a function of the percentage of pS in the systems (pure pS monolayer in light blue). The experiments were performed using Tris HCl buffer at pH 7 and were done in duplicate. Values of π were given with a standard deviation on duplicate measurements of ± 0.2 mN/m.

**Figure 3** 5x5 µm² and 1x1 µm² AFM topographic images of A) GL, B) $GL_{50}/DPPC_{50}$, and C) $GL_{45}/DPPC_{45}/pS_{10}$ model monolayers. The height profiles were performed on a cross-section of the 1x1 µm² image. The Langmuir films were transfer at a surface pressure of 20 ± 0.5 mN/m on a mica plate using the Langmuir Blodgett method. Experiments were performed in a Tris HCl buffer at pH 7 and done in duplicate.

**Figure 4** 5x5 µm² AFM topographic images of A) $MGDG_{50}/DPPC_{50}$, B) $DGDG_{50}/DPPC_{50}$, C) $MGDG_{30}/DPPC_{60}/pS_{10}$, and D) $DGDG_{30}/DPPC_{60}/pS_{10}$ monolayers. Zooms to 1x1 µm² were performed on samples C) and D) to allow visualization of defects in condensed areas. The height profiles were performed on three different cross-sections of the 5x5 µm² image. The Langmuir films were transfer at a surface pressure of 20 ± 0.5 mN/m on a mica plate using the Langmuir Blodgett method. The ellipsometric angle value at 20 mN/m was reported to compare the thickness between the four monolayers. Experiments were performed in a Tris HCl buffer at pH 7 and done in duplicate.

**Figure 5** SAXS patterns of the model systems recorded at 20 ± 0.5°C. A) GL/DPPC systems at different ratios: 33:67 mol/mol (black curve), 50:50 mol/mol (blue curve) and 67:33 mol/mol (green curve). B) DGDG/DPPC/pS (45:45:10 mol/mol/mol, green curve), GL/DPPC/pS (45:45:10 mol/mol/mol, black curve), MGDG/DPPC/pS (45:45:10 mol/mol/mol, blue curve)

662 **Figure 1**

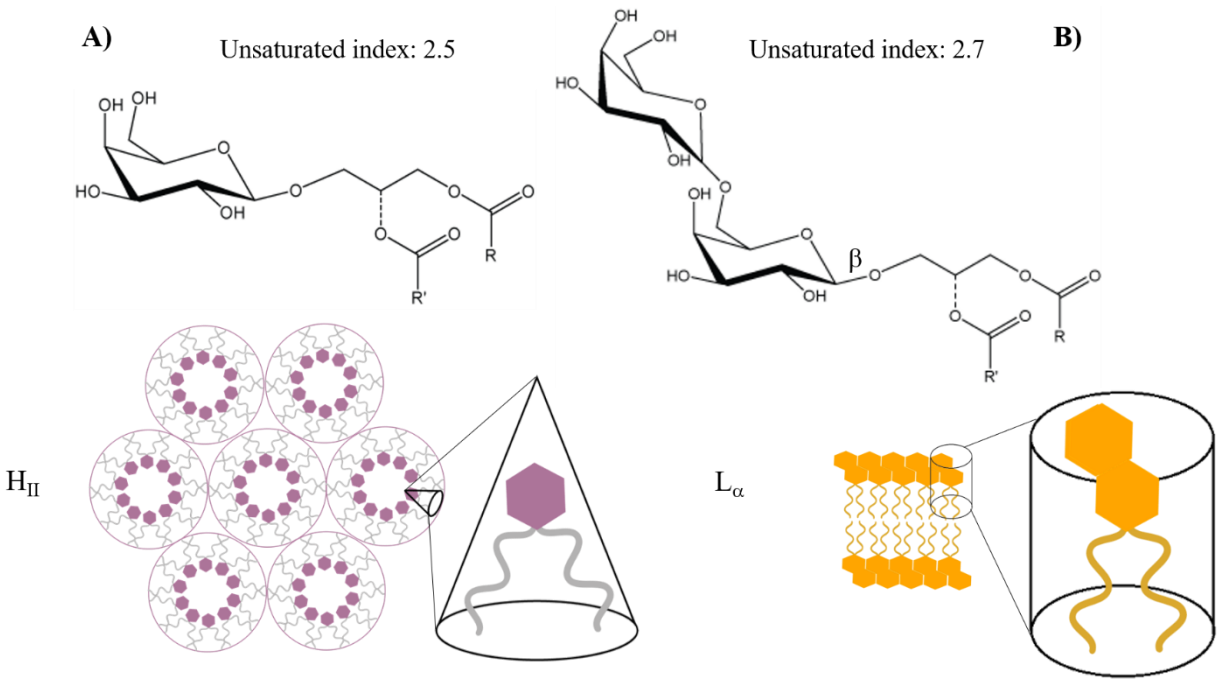


663

664

**Figure 2**

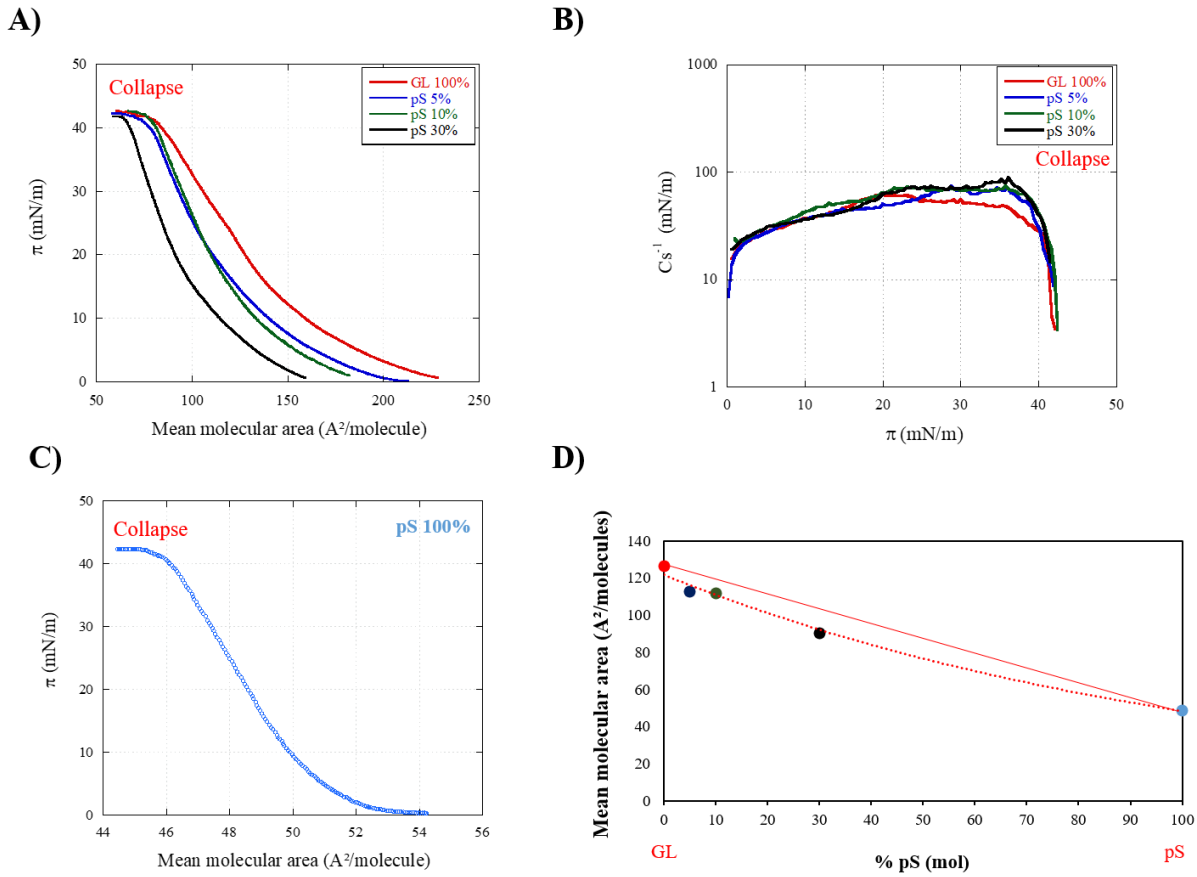
A)
Collapse
GL 100%
pS 5%
pS 10%
pS 30%
π (mN/m)
Mean molecular area (A²/molecule)
B)
GL 100%
pS 5%
pS 10%
pS 30%
Collapse
Cs⁻¹ (mN/m)
π (mN/m)
C)
Collapse
pS 100%
π (mN/m)
Mean molecular area (A²/molecule)
D)
Mean molecular area (A²/molecules)
GL
% pS (mol)
pS

**Figure 3**

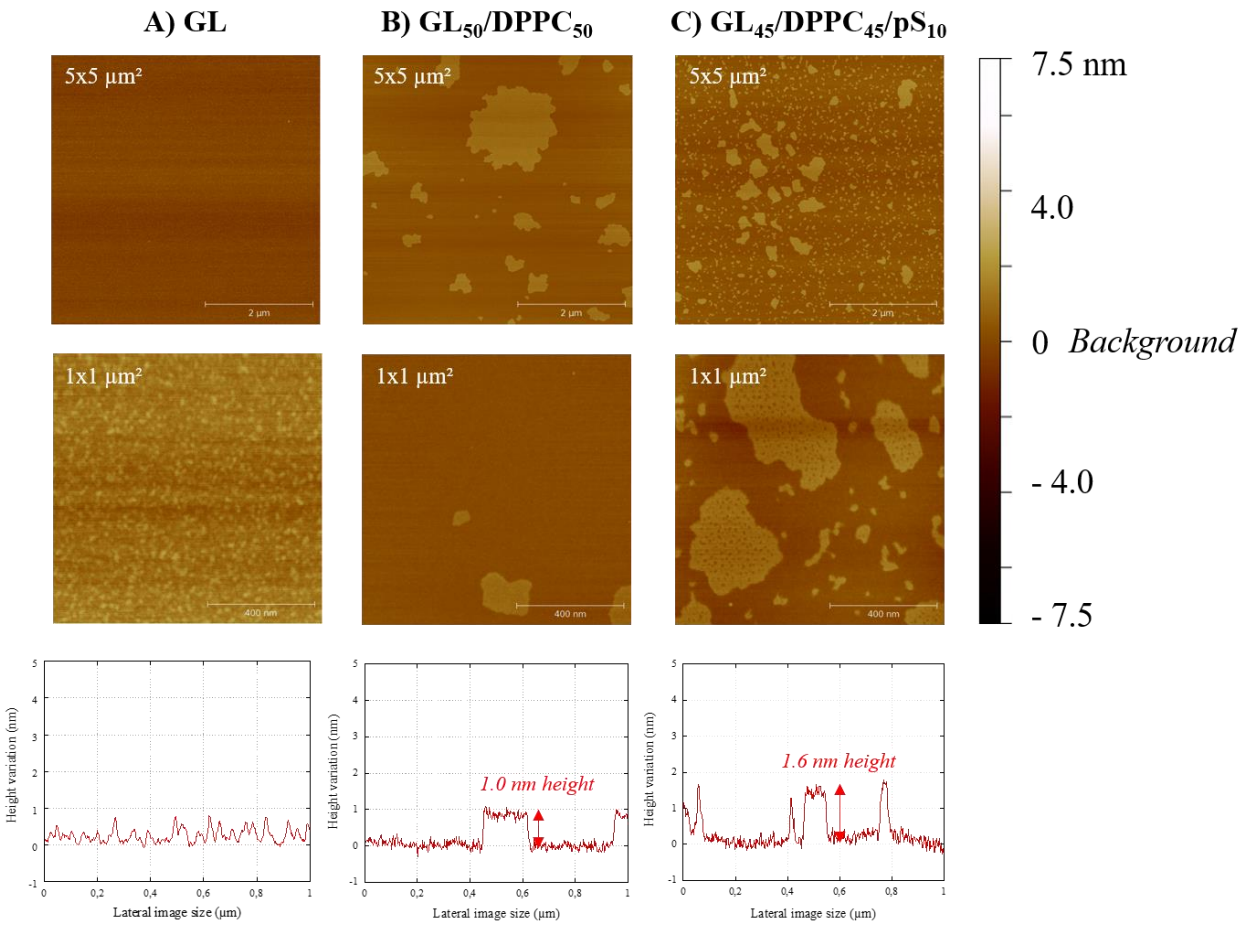
A) GL
B) GL50/DPPC50
C) GL45/DPPC45/pS10
5x5 µm²
1x1 µm²
2 µm
400 nm
7.5 nm
4.0
0 Background
- 4.0
- 7.5
Height variation (nm)
Lateral image size (µm)
1.0 nm height
1.6 nm height

671 **Figure 4**

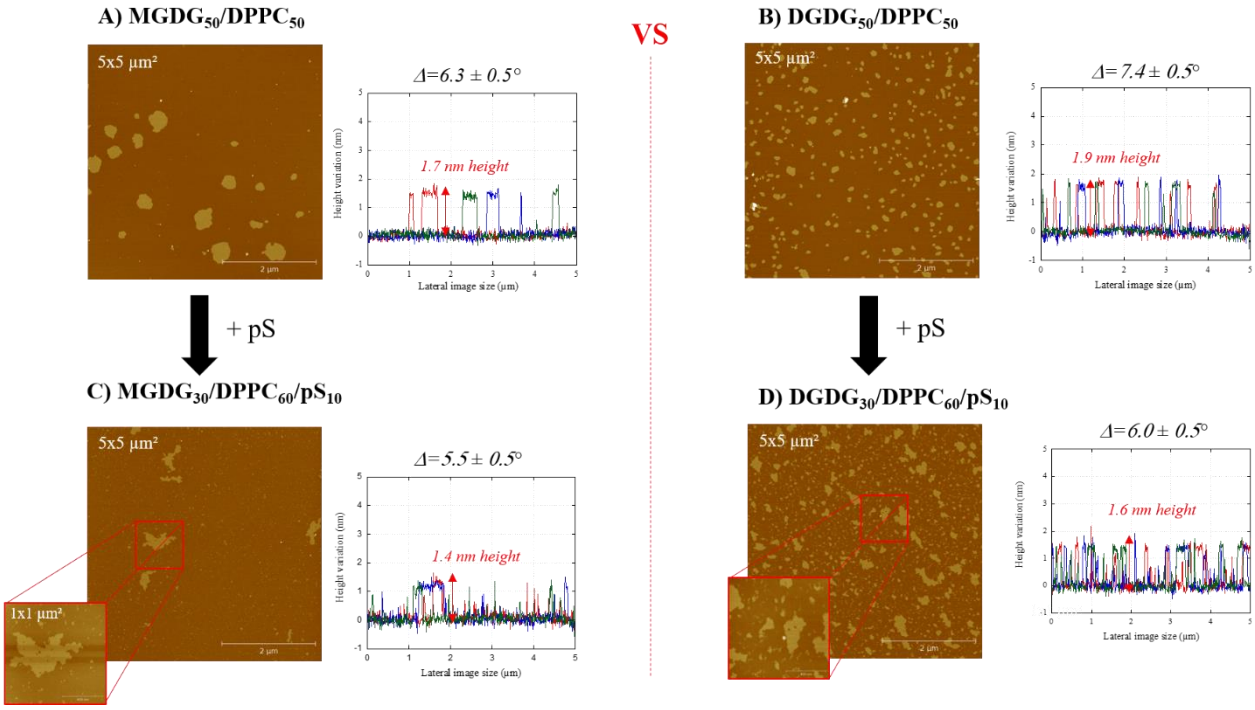


672

673

674 **Figure 5**

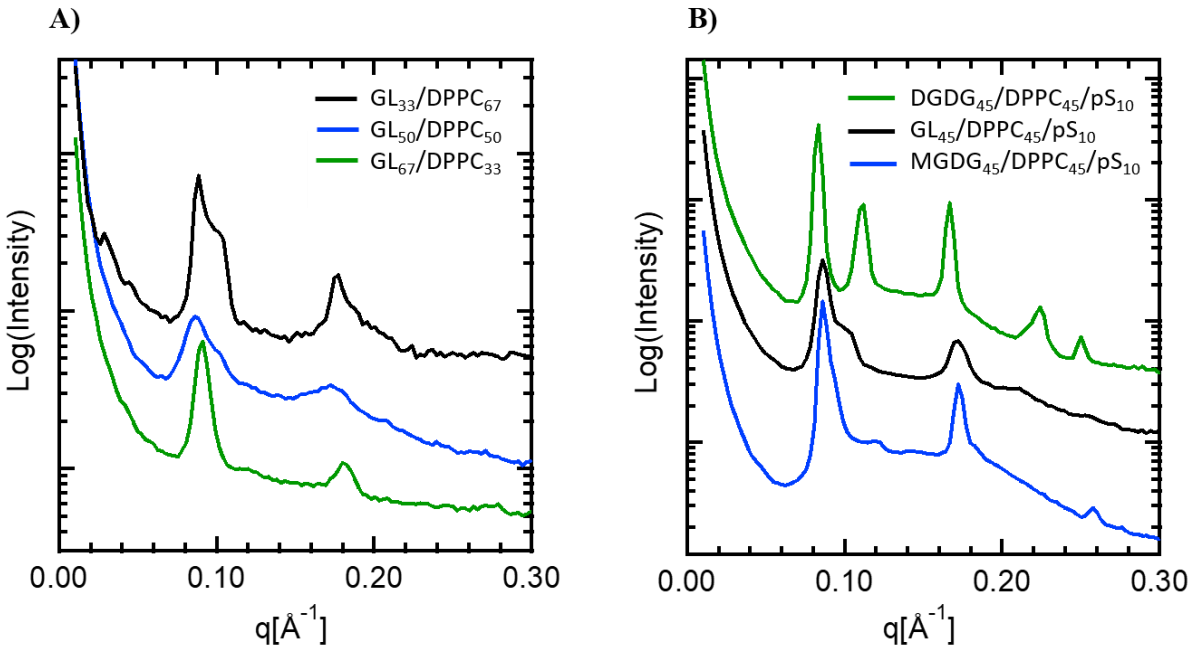


675

676

## TABLES

**Table 1** - Molar composition of mixed Langmuir monolayers used as model membranes

| | Monolayer composition |
|---|---|
| GL | MGDG/DGDG 60:40 mol/mol |
| $GL_{50}/DPPC_{50}$ | MGDG/DGDG/DPPC 30:20:50 mol/mol/mol |
| $GL_{45}/DPPC_{45}/pS_{10}$ | MGDG/DGDG/DPPC/pS 27:18:45:10 mol/mol/mol/mol |

*pS: β-sitosterol, campesterol, brassicasterol 50:40:10 mol/mol/mol*

**Table 2** - Values of π (mN/m), Δ (°) and limiting molecular area (Å²/molecule) at the collapse of mixed GL, DPPC and pS monolayers

| Monolayer composition | π (mN/m) | Δ (°) | Limiting area (Å²/molecule) |
|---|---|---|---|
| **(1) GL** | 39.9 ± 0.2 | 7.3 ± 0.5 | 81.0 ± 0.6 |
| **(2) DPPC** | 55.3 ± 0.2 | 10.8 ± 0.5 | 44.1 ± 0.7 |
| **(3) $GL_{50}/DPPC_{50}$** | 44.1 ± 0.2 | 8.9 ± 0.5 | 60.4 ± 1.0 |
| **(4) $GL_{90}/pS_{10}$** | 41.1 ± 0.1 | 8.2 ± 0.5 | 79.5 ± 0.9 |
| **(5) $GL_{45}/DPPC_{45}/pS_{10}$** | 44.4 ± 0.2 | 8.6 ± 0.5 | 55.0 ± 1.7 |

± stands for calculated standard deviation on duplicated measurement; for Δ, since the system/instrumentation error is ± 0.5°, calculated SD ≤ 0.5 were minored by this instrumentation error.

687 **Table 3** - Ellipsometric angle values of the lipid films at a surface pressure of 20 mN/m at the

688 air/water interface

| Monolayer composition | Δ (°) |
|---|---|
| MGDG | 6.3 ± 0.5 |
| DGDG | 7.5 ± 0.5 |
| **(1) GL** | **7.5** ± 0.5 |
| **(2) $GL_{50}/DPPC_{50}$** | **7.1** ± 0.5 |
| **(3) $GL_{45}/DPPC_{45}/pS_{10}$** | **7.0** ± 0.5 |

± stands for calculated standard deviation on duplicated measurement; the system/instrumentation error is ± 0.5°. Calculated SD ≤ 0.5 were minored by this instrumentation error.

689

690